Multi-shell diffusion imaging reveals sex-specific trajectories of early white matter degeneration in normal aging

Abbreviated title: Sex-specific trajectories of degeneration in aging

Nicola Toschi[1,2], Rebeca Arrais Gisbert[3], Luca Passamonti[4], Santiago Canals[3], Silvia De Santis[3,5*]

[1]Athinoula A. Martinos Center for Biomedical Imaging and Harvard Medical School, Boston, MA, USA.

[2]Department of Biomedicine and Prevention, University of Rome Tor Vergata, Rome, Italy

[3]Instituto de Neurociencias de Alicante (CSIC-UMH), San Juan de Alicante, Spain

[4]Department of Clinical Neurosciences, University of Cambridge, Cambridge, UK

[5]Cardiff University Brain Research Imaging Centre (CUBRIC), Cardiff University, Cardiff, UK

[*]corresponding Author. E-mail: dsilvia@umh.es

Number of pages: 26

Number of figures/tables: 7/0

Number of words for abstract/introduction/discussion: 172/786/1660

Conflict of interest: The authors declare no competing financial interests

Acknowledgments:

Dr. De Santis is supported by a NARSAD Young Investigator Grant (Grant #25104) and by the European Research Council through a Marie Skłodowska-Curie Individual Fellowship. LP is supported by the Medical Research Council (MRC), UK (MR/P01271X/1).

Abstract

During aging, human white matter (WM) is subject to dynamic structural changes which have a deep impact on healthy and pathological evolution of the brain through the lifespan; characterizing this pattern is of key importance for understanding brain development, maturation and aging as well as for studying its pathological alterations. Diffusion Magnetic Resonance Imaging (MRI) can provide a quantitative assessment of the white-matter microstructural organization that characterizes these trajectories. Here, we use both conventional and advanced diffusion MRI in a cohort of 91 individuals (age range: 13-62) to study region- and sex-specific features of WM micro-structural integrity in healthy aging. We focus on the age at which microstructural imaging parameters invert their development trend as the timepoint which marks the onset of microstructural decline in WM. Importantly, our results indicate that age-related brain changes begin earlier in males than females and affect more frontal regions - in accordance with evolutionary theories and numerous evidences across non-MRI domains. Advanced diffusion MRI reveals age-related WM modifications patterns which cannot be detected using conventional DTI.

Keywords: Aging, WM, Microstructural integrity, Diffusion MRI, CHARMED, sex differences

1. Introduction

In recent years, in addition to the well-known role of brain white matter (WM) in a number of degenerative and psychiatric disorders (Goveas et al., 2015), its key importance in nearly every aspect of healthy cognition has been widely recognized (Filley and Fields, 2012). During the lifespan, WM evolves across multiple spatial scales, ranging from molecular to macroscopic. In humans, myelination of axonal fibers begins during gestation and continues into adulthood through the second-third decades of life and possibly beyond (Yakovlev and Lecours, 1967; Miller et al., 2012). Concurrently, aging causes a degradation of WM tissue integrity mostly connected to myelin breakdown (Bartzokis et al., 2010) and accompanied by low-grade chronic inflammation (Franceschi et al., 2007). Characterizing WM evolution across the lifespan in the healthy population is therefore critical for understanding brain development, maturation and aging as well as and for studying its pathological alterations.

Diffusion tensor imaging (DTI, Basser et a., 1994) is a non-invasive *in vivo* method for characterizing WM, which provides a quantitative assessment of its microstructural organization. DTI is sensitive to the distribution of the barriers encountered by water molecular diffusion within biological tissue (mostly axonal membranes and myelin, according to Beaulieu et al., 1994). DTI studies across the lifespan have shown a progressive increase in fractional anisotropy (FA) during the first two decades of life, followed by a decrease which progresses at a faster rate after 60 years (de Groot et al., 2016). This pattern is believed to reflect axonal and myelin changes (Kemper, 1994).

WM microstructure maturation during the lifespan is heterogeneous across brain regions, and there is converging evidence for an anteroposterior gradient in age-related WM changes (Davis et al. 2009). This is in keeping with the hypothesis that neuronal

vulnerability with aging is higher in the prefrontal cortex (PFC) (Mattson and Magnus, 2006). This pattern is particularly evident in the corpus callosum, the major inter-hemispheric WM pathway in the brain, in which increased vulnerability to aging is more prominent in the genu (anterior part of the corpus callosum) as compared to the splenium (posterior corpus callosum) (Sullivan et al., 2010; Fan et al., 2019).

While sex differences in WM have been extensively reported using DTI (Kanaan et al. 2012), interactions between sex and age reported to date are either no significant (Sullivan and Pfefferbaum 2006) or small/inconsistent (Cox et al., 2015). However, it is reasonable to believe that WM trajectories are also sex-specific. Animal studies showed that age-related changes in myelination are more prominent in males than females (Yang et al. 2008), and studies examining cognitive and emotion processing consistently highlighted that age-related decline begins earlier in men as compared to women (Gur and Gur, 2002). Notably, brain metabolism (as assessed via positron emission tomography) has been reported to be on average, a few years "younger" in females than in males (Goyal et al., 2019). Imaging results analyzing large cohorts point at the existence of structural and functional gender differences in adults (Ritchie et al., 2018; Lotze et al., 2019). Evolutionary theories also support the existence of sex differences in aging trajectories, which could be linked to diverse factors that cause sex-specific mortality (Chen and Maklakov, 2014). Clarifying this interaction is therefore a key prerequisite to employ diffusion MRI measures as reliable biomarkers. In this context, an important factor in partially explaining the lack of sex-specific diffusion MRI findings in aging could be the widespread use of conventional DTI-derived measures, which lack sufficient sensitivity to characterize axonal microstructural integrity (Beaulieu, 2002; De Santis et al., 2014).

Advanced multi-shell diffusion-weighted imaging methods, including the Composite Hindered and Restricted Model of Diffusion (CHARMED; Assaf and Basser, 2005), address these limitations by explicitly separating intra- and extra-axonal diffusion compartments and thereby estimating the restricted signal fraction (FR). Importantly, the CHARMED model explores very high diffusion weightings or b-values, maximizing the sensitivity towards axonal integrity, and accounts for crossing fibers (up to three populations in each voxel). It was recently shown (De Santis et al., 2017, De Santis et al., 2019, Toschi et al. 2019) that FR is more sensitive to axonal integrity as compared to DTI.

Previous studies have looked into the benefits of advanced multi-shell diffusion at relatively low b-value for characterizing different aspects of brain microstructure in normal aging (Billiet et al. 2015; Cox et al., 2015; Nazeri et al., 2015; Beniteza et al. 2018; Slater et al., 2019), but no-one thus far has examined the age at which age-related changes begin, or the possibility that sex-related effects may drive age dependent changes in WM using a high b-value approach. Therefore, in this study we hypothesized that advanced diffusion MRI would disclose regional and sex-specific patterns of WM changes that have thus far eluded conventional DTI-based assessment. Specifically, we expected that men would show an earlier onset of age-related degradation, especially in prefrontal WM.

2. Methods

2.1 Data Acquisition

We employed the publicly available National Taiwan University Diffusion Spectrum Imaging MRI dataset, composed of n=91 participants in the range 13-62 (Yeh et al., 2011).

The participant population comprised 49 males (mean age 32+/-13 years) and 42 females (mean age 33 +/- 13 years). No statistically significant age difference was found between sexes (P=0.555, two-sided two sample t-test; age histograms in Supplementary Fig.1). Participants did not report any history of neurological or mental disorders, nor were they taking psychotropic medication concurrent with MR imaging. Diffusion weighted images were acquired on a Siemens Trio scanner using a 2D EPI diffusion sequence (ep2d_diff_MGH-DSI2_050922) with the following parameters: TE=142 ms; TR=9100 ms; in-plane resolution 2.9 mm; slice thickness 2.9 mm; matrix 128X128, 49 slices. A multi-shell gradient scheme was used with a total of 203 grid sampling points as proposed by an optimization study (Kuo et al., 2008), with a maximum b-value of 6000 s/mm^2. The gradient orientations were distributed in each b-value shell in the following way: 6 orientations for b=62 s/mm^2, 12 for b=923 s/mm^2, 8 for b=1385 s/mm^2, 6 for b=1846 s/mm^2, 24 for b=2300 s/mm^2, 24 for b=2800 s/mm^2, 12 for 3700 s/mm^2, 30 for b=4100 s/mm^2, 24 for b=4600 s/mm^2, 24 for b=5100 s/mm^2, 8 for 5500 s/mm^2, and 24 for b=6000 s/mm^2. The total scanning time for all diffusion MRI data was 45 min.

2.2 Data Processing

Diffusion pre-processing included motion and eddy current correction followed by b-matrix reorientation and was performed using the software ExploreDTI (v.4.8.4, http://www.exploredti.com/) (Leemans et al., 2009). The 33 gradient orientation belonging to lower b-value shells (up to b=1846 s/mm^2) and the b0 were used to run DTI analysis using ExploreDTI. In this analysis, the tensor model was fitted using a Robust Estimation of Tensors by Outlier Rejection approach (Chang et al., 2005), after which the following maps were computed for each participant: fractional anisotropy (FA), mean diffusivity (MD), axial diffusivity (AD) and radial diffusivity (RD). Subsequently, all shells and all images were employed to fit the CHARMED model (Assaf and Basser,

2005) using a non-linear least square fitting routine implemented as in-house software written in MATLAB R2015b (The MathWorks, Natick, MA, USA). CHARMED separately models the contribution of the signal originating from the extra-axonal space (that undergoes hindered diffusion, described as a tensor) and that originating from the intra-axonal space (that undergoes restricted diffusion, described using the expression for restricted diffusion in cylinders proposed by Van Gelderen et al., 1994), as schematized in Figure 1. We then estimated the total signal fraction of the restricted (i.e. modeled as intra-axonal) diffusion compartment FR, the orientation of the restricted compartment, the diffusivity of the restricted compartment, the extra-axonal tensor (without relying on the tortuosity approximation as defined in Szafer et al. 1995) and a noise term, for a total of 19 parameters. The initialization values fed to the fitting routine were: FR=0.3 (range 0-1), orientation [0 pi/2] (range 0 pi/2), diffusivity=1*10-3m2/s (range 0.1-5) for each fiber, diffusion tensor [0.3 0.3 1.2 0 0 0] (range [0.1 0.1 0.1 -3 -3 -3] - [5 5 5 3 3 3]), and noise 0 (range 0-1). All fit parameters can vary within their physically plausible range, i.e., diffusivities must be positive and smaller or equal to the diffusivity of free water. FR maps were generated for all participants for subsequent analysis.

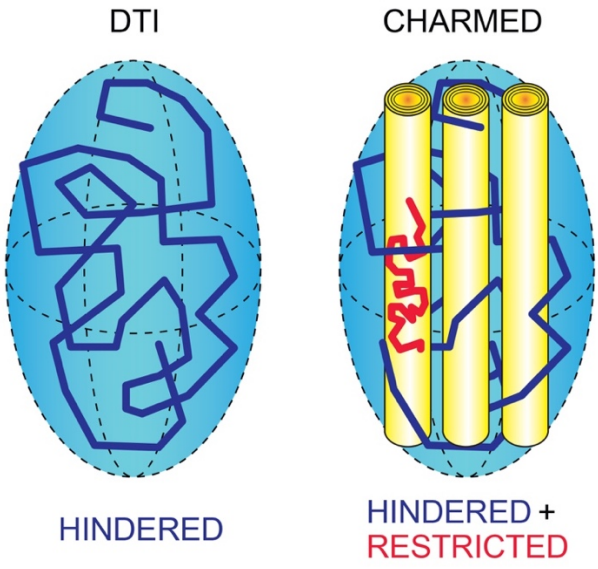

Figure 1*: While DTI models the diffusion as hindered (left), CHARMED (right) models the signal as originating in part from the extra-axonal space, which undergoes hindered diffusion (in blue), and in part intra-axonal space, which undergoes restricted diffusion (in red) using two different analytical probability distribution functions (Assaf et al., 2005).*

2.3 Whole-brain diffusion parameter extraction

To perform whole brain analysis, we combined the normalization and skeletonization routine included in FSL (Smith et sl. 2006) with an automatic region of interest (ROI)-based aggregation based on WM labelling in standard space (JHU ICBM DTI 81 Atlas by Mori et al. 2008, also available in FSL, total 50 ROIs) as previously described (De Santis et al., 2012). This allows to simultaneously minimize registration- and interpolation-related biases (through skeletonization) and increase sensitivity through ROI-wise averaging (Coutu et al. 2014). In detail, FA maps computed from the DTI model were fed into an in-house modified version of the Tract-Based Spatial Statistics (TBSS) routine (Smith et al., 2006), in which the normalization to MNI standard space is performed using more accurate registration tools (ANTs package, Klein et al., 2009). The warp fields were then employed to transform all other images into a common (MNI) space, in which the skeletonization transform computed above is applied to all other maps. After skeleton extraction, the skeleton is combined with the ICBM DTI 81 Atlas, and for all participants and parameters, mean values are calculated for each parameter in each ROI belonging to the WM parcellation.

2.4 Statistical analysis

2.4.1 Modeling of onset age

We assess the age at which the WM microstructural imaging parameters (conventional i.e., FA, MD, AD and RD, and advanced, FR) invert their development trend, and interpret this age as a 'turning point' in microstructural changes: we refer to this as "onset

age". In a first analysis, we aimed to characterize the spatial distribution of the onset age. Previous studies have used a quadratic regression order to model the non-monotonic microstructural evolution between 1) adolescence and maturity (increasing anisotropy, decreasing diffusivities) and 2) maturity and older adult age (decreasing anisotropy, increasing diffusivities) (Billiet et al., 2015; Xie et al., 2016). Therefore, for each ROI we modeled microstructural parameters across participants as follows:

(1) $P=A+B*sex+C*age+D*age^2$ (model 1)

where P is the ROI-averaged microstructure parameter $P = \{FA, MD, RD, AD, FR\}$ and A, B, C and D are the regression coefficients. Here the onset age (i.e. peak of the parabola, see Figure 2A) can be calculated as $-C/2D$, and the sign of the regression coefficient D indicates the direction of the trend (positive: upward parabola, negative: downward parabola). This first model accounts for sex differences in microstructural parameter values while assuming a unique onset age across sexes. The model-wise p-value was corrected for multiple comparisons across ROIs using a false discovery rate (FDR) approach (alpha = 0.05). $P<0.05$ was considered statistically significant. In regions where significant effects were found, the skeleton was inflated for visualization purposes using the routine "tbss_fill" included in FSL.

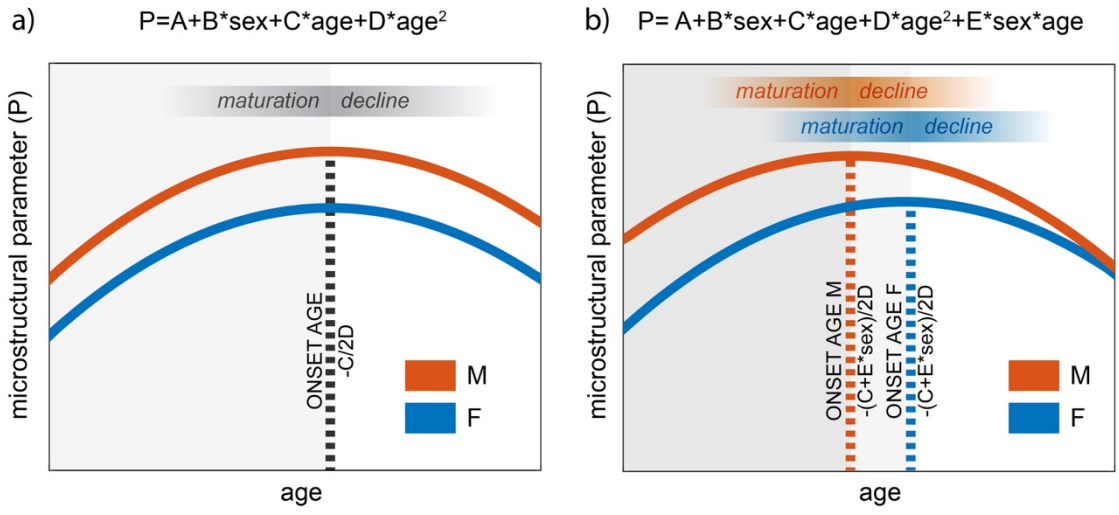

Figure 2*. ROI-wise regression models across participants. a) Quadratic model with age and sex effect, but no interaction between age and sex (see 2.4.1). This model assumes a unique onset age across sexes. b) Quadratic model with sex age and effect as well as sex * age interaction (see 2.4.4). This model allows for different, sex-specific onset ages.*

2.4.2 Spatial distribution of onset age

To investigate spatial trends (anterior-posterior: A-P; inferior-superior: I-S, left-right: L-R) in onset age across the brain independently of sex, the relationships between onset age estimated through model 1 and A-P, I-S and L-R coordinates of the ROI-wise geometric centers (i.e. average position of each ROI within the brain) were tested using linear regression. $P<0.05$ was considered statistically significant. This analysis was performed in all ROIs in which the quadratic dependence on age (coefficient *D* in model 1) was found to be statistically significant ($P<0.05$).

2.4.3 Comparison of onset age across indices

In order to compare the onset age across indices, we employed a Friedman test for repeated measures (factor: index), followed by post-hoc comparison and Bonferroni correction for multiple comparisons across indices. $P<0.05$ was considered significant. As above, this analysis was performed in all ROIs in which the quadratic dependence on age (coefficient D in model 1) was found to be statistically significant ($P<0.05$).

2.4.4 Sex - onset age interaction

In a second analysis, we aimed at exploring a putative sex-related difference in onset age. To this end, for each ROI we modelled microstructural parameters using an additional interaction term as follow:

(1) $P= A+B*sex+C*age+D*age^2+E*sex*age$ (model 2)

where *P* is the ROI-averaged microstructure parameter as above, and *A, B, C, D* and *E* are the regression coefficients, from which the (sex-specific) onset age can be calculated as $-(C+E*sex)/2D$ (see Figure 2B). This second model allows for sex differences in

microstructural parameter values as well as for sex-specific onset ages. For each parameter, onset age was compared between sexes using a Wilcoxon signed-rank test, and $P<0.05$ was considered statistically significant.

3. Results

3.1 Quadratic dependence between imaging parameters and age

As a preliminary step, we employed a model selection criterion (Bayesian Information Criterion (BIC)) for each imaging parameter and for each ROI to compare between linear and quadratic models. Across all parameters and ROIs, the quadratic model is consistently selected by the BIC, except in 3 ROIs for FR, where a linear model is chosen (medial lemniscus, inferior cerebellar peduncle, tapetum). Accordingly, these 3 data points were excluded from following analyses. Figure 3 shows the portion of the skeleton in which the quadratic regression term (model 1) was found to be statistically significant for FA (22% of ROIs), MD (54% of ROIs) and FR (64% of ROIs). P-values are reported in Supplementary Table 1. Notably, the WM afferences to the frontal lobe show a quadratic dependence on age for FR only. All results for AD and RD are reported as supplementary materials (Figure S2 and S3).

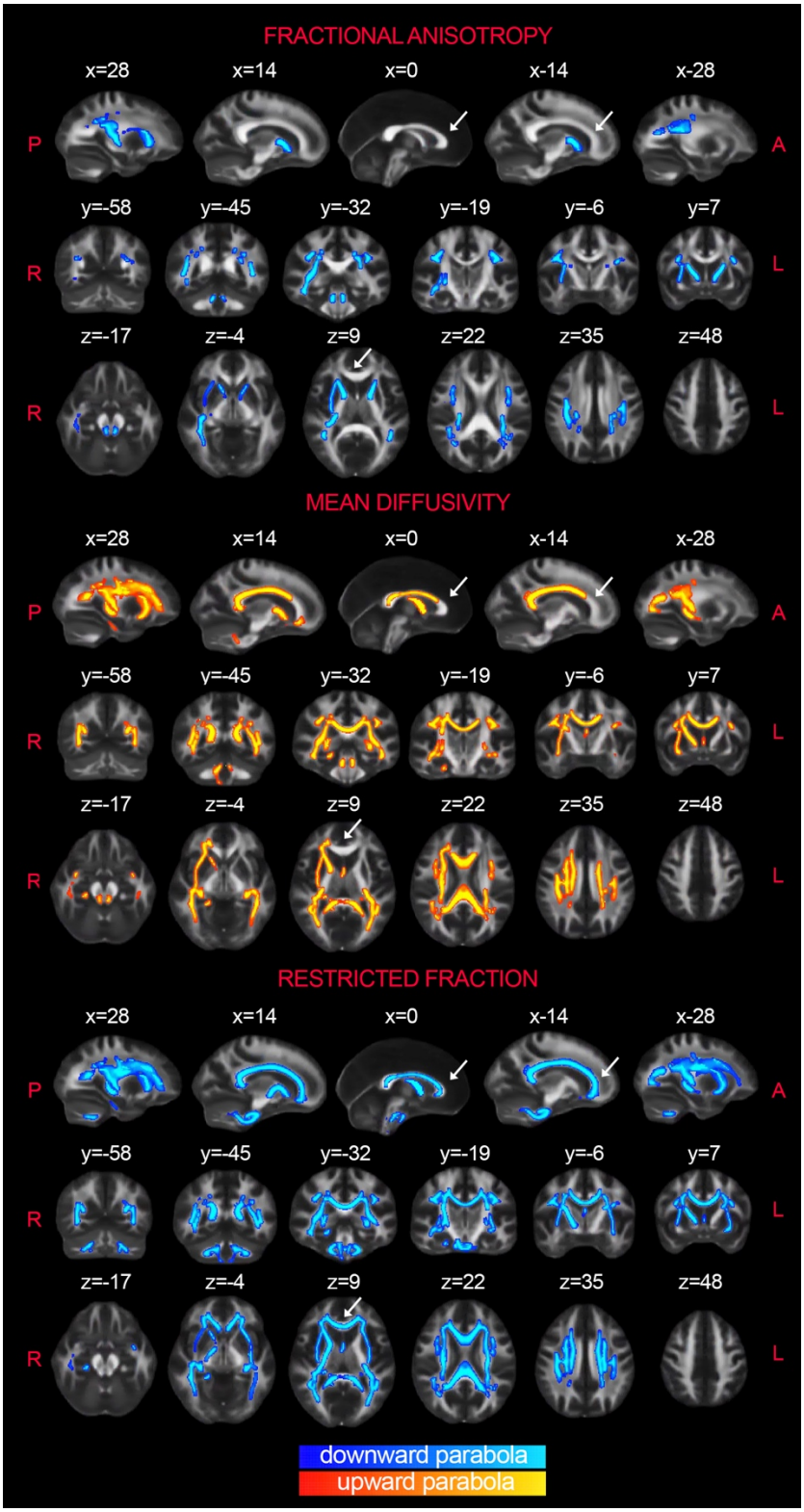

Figure 3. *Portion of the parcellated skeleton where a significant quadratic dependence between the microstructural parameter and age was found in model 1. Color indicates the sign of the regression coefficient: red-yellow indicates a positive coefficient (upward parabola), blue-lightblue indicated a negative coefficient (downward parabola). FR is the parameter for which the quadratic trend is significant in the highest number of regions (64%), and notably in the frontal WM (white arrow).*

3.2 Spatial distribution of onset age

Regression analysis for all ROIs (onset age against position of ROI in the brain) revealed a significant age onset gradient for MD and FR indices in both A-P and I-S directions (Fig. 4). No significant L-R gradients were found in any indices.

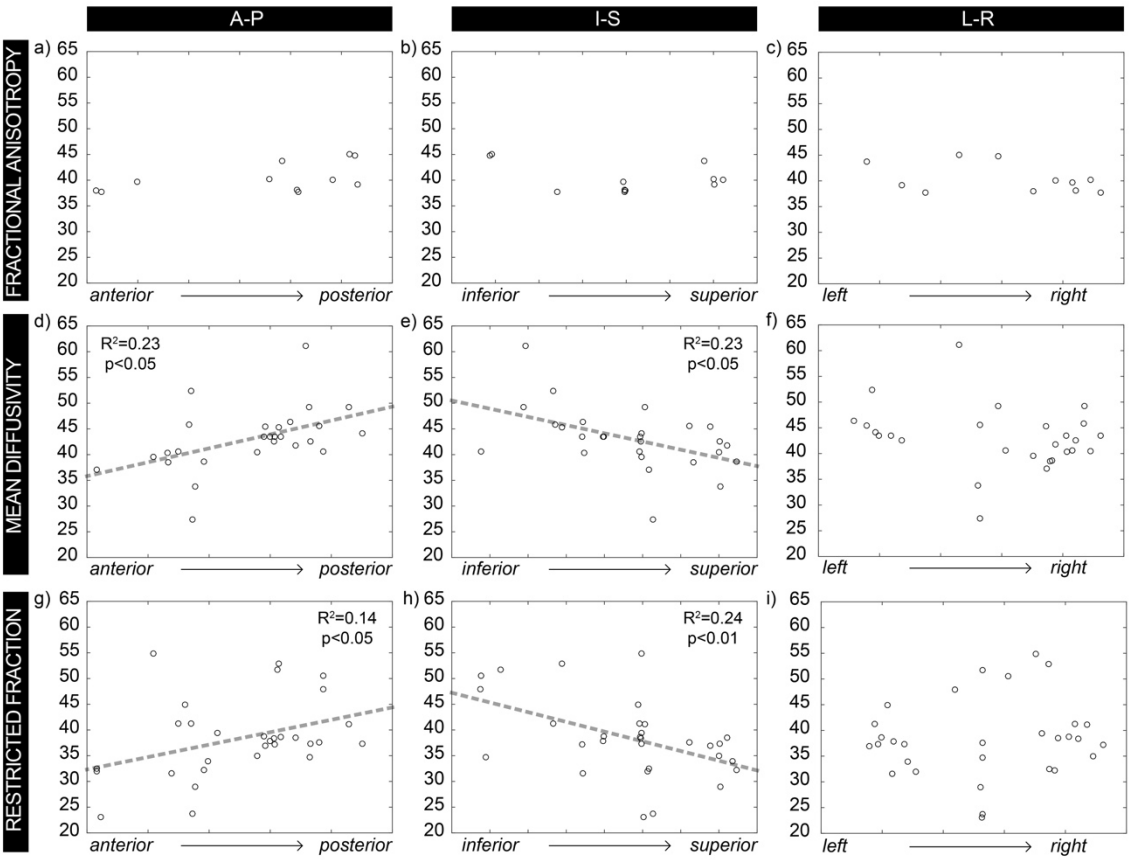

Figure 4*. a)-i): Onset age as a function of position in all ROIs where the quadratic dependence on age was statistically significant in model 1, plotted as a function of the A-P (left), I-S (center) and L-R (right) coordinates of the geometric center of each ROI. Whenever the linear regression is statistically significant, the R^2-value, p-value and the regression line (dashed grey line) are reported.*

As an example, and for visualization purposes, Fig. 5 depicts three specific ROIs belonging to the corpus callosum, along with the corresponding scatterplots and estimated quadratic regression curves for FA, MD and FR. The A-P gradient in onset age is clearly visible in all corpus callosum for FR and partially (body and splenium) for MD.

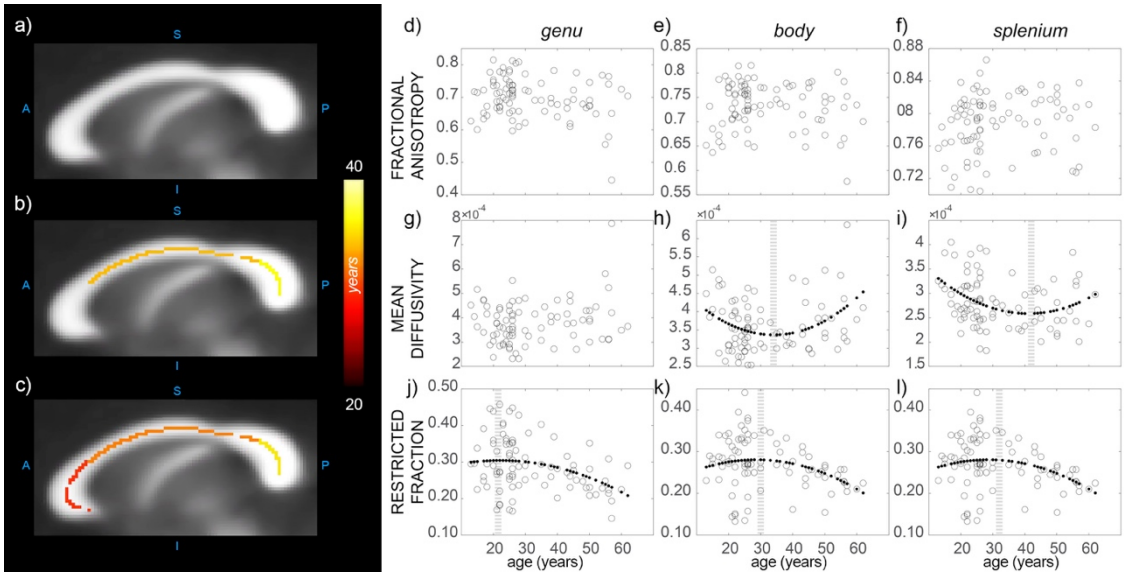

Figure 5. *a) Onset age in the corpus callosum estimated from FA (a), MD (b) and FR (c); d)-f) scatterplots of FA vs. age in the three ROIs of the corpus callosum (splenium, body and genu, respectively); g)-i) scatterplots of MD vs. age; j)-l) scatterplots of FR vs. age. When the quadratic coefficient D in model 1 was statistically significant, the fitted parabola is shown as a dotted line. The vertical dashed line highlights the peak of the parabola, whose position indicates the onset age.*

3.3 Comparison of onset age across indices

Figure 6 summarizes the onset age for all microstructural parameters, including all ROIs in which the quadratic dependence on age was statistically significant in model 1. Onset age estimated by FR is notably lower than onset age estimated by all other parameters in a large number of ROIs. The Friedman test for repeated measured shows a significant effect of index (P=0.03). Overall, median onset age (across ROIs and independent of sex) estimated by FR (37.7 years) was significantly lower (p=0.024) than median onset age estimated by MD (43.5 years). When calculated only in ROIs in which the quadratic model was significant across all indices (right internal capsule, left corona radiata, right thalamic radiation, right external capsule, right cingulum, superior longitudinal fasciculus bilaterally), the same difference in median onset age is found across indices: 39.4 years for FA, 42.2 years for MD and 37.9 years for FR. Location of the onset age is reported in Supplementary material (Figure S4).

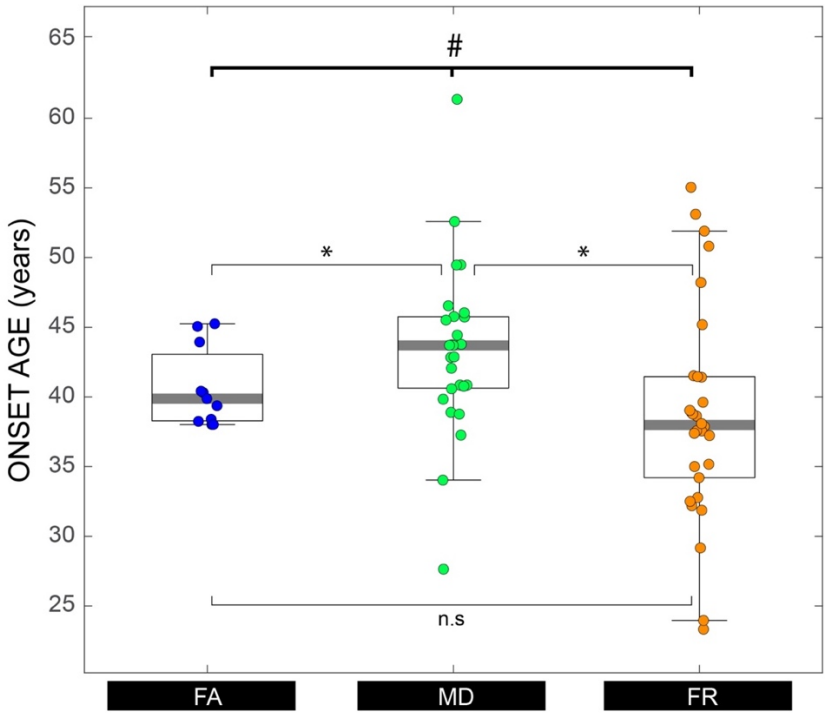

***Figure 6**. Onset age calculated for all microstructural parameters in all ROIs in which the quadratic dependence on age is statistically significant in model 1. Median values are 39.6 years for FA, 43.5 years for MD and 37.7 years for FR. Thick bracket and hashtag refer to Friedman statistic, thin brackets and asterisks refer to post-hoc comparisons between indices. Thick horizontal lines: medians; boxes: quartiles; whiskers: extremes.*

3.4 Sex and sex - age interaction

Sex is significantly associated with FA in 2 regions and with FR in 34 ROIs, with men displaying higher mean value of FA (0.63+/-0.12 vs 0.61+/-0.11) and FR (0.34+/-0.06 vs 0.31+/-0.06) compared to women. FR shows significant age-sex interactions in 14 ROIs (Fig. 7), notably: the corpus callosum (Fig. 7b), the corona radiata, the sagittal stratum, the inferior fronto-occipital fasciculus and inferior longitudinal fasciculus. Both FA and MD show significant age-sex interactions in one ROI each (the left anterior corona radiata and in the fornix, respectively). P-values are reported in Supplementary Table 1. In all ROIs where the quadratic term of model 2 is significant, the decline starts earlier in males, with an average age across ROIs (calculated from model 2) for FR of 29.1 years for males

and 43.4 years for females. Difference in onset age across sexes is reported in Supplementary Figure 5.

Global metrics for FA, MD and FR calculated in the whole skeleton show the same trend observed in ROIs, as reported in Supplementary Figure 6. The presence of an age-sex interaction may explain the high variability in the FR onset age calculated using model 1 (Fig. 6). The Wilcoxon signed-rank test confirmed that the ages are significantly different ($p<0.0001$). The median onset ages in males and females for FR is shown in the box-whisker plot included in Fig. 7c. The same results for DTI indices are reported in Supplementary Figure 7.

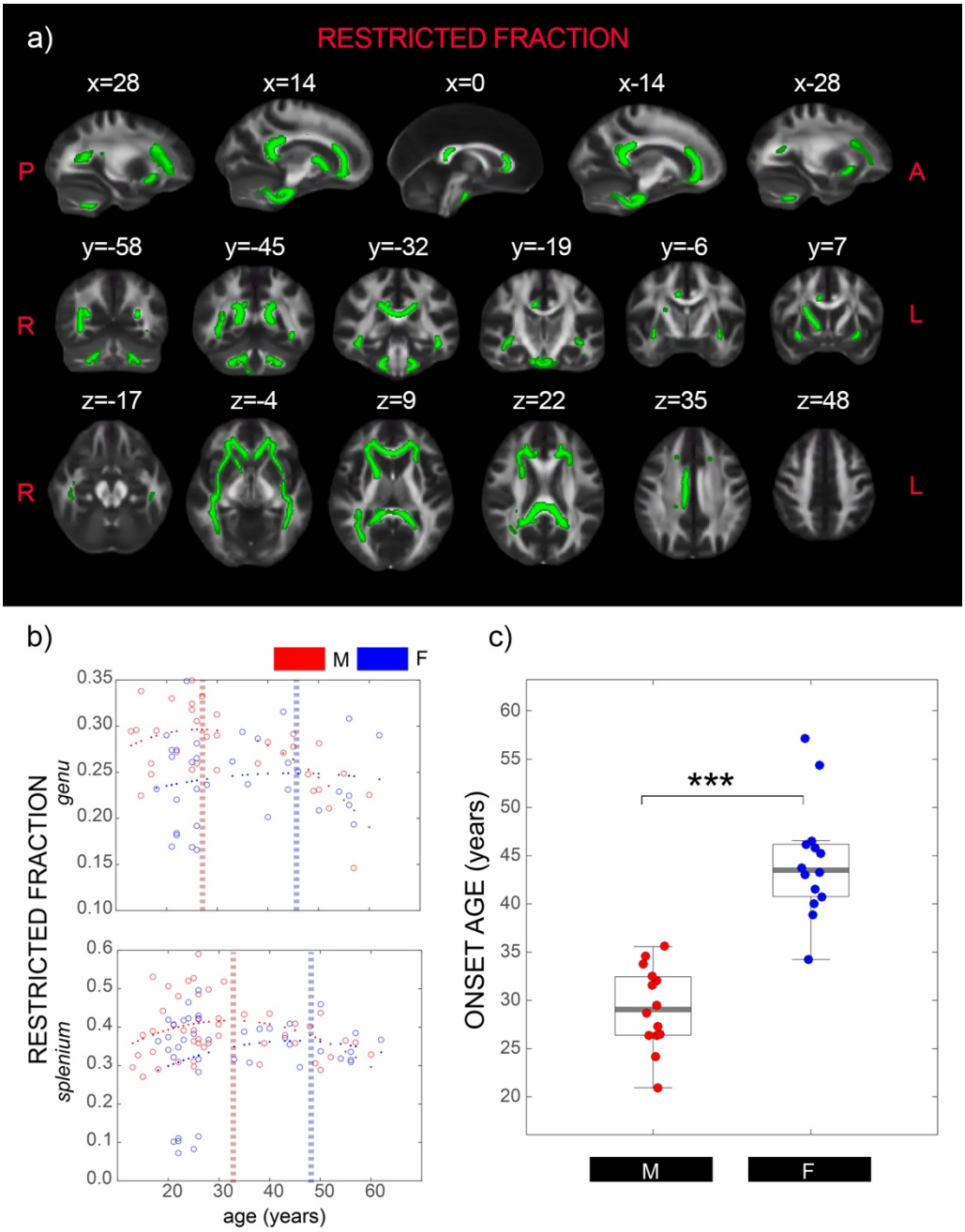

***Figure** 7. a) Portion of the parcellated skeleton where the sex * age term was found to be statistically significant in model 2 for FR. The same analysis for DTI measures is reported in the supplementary material. b) Scatterplots of FR vs. age in the two ROIs of the corpus callosum (splenium, upper panel, and genu, lower panel) with quadratic model and peak, reported in red for males and in blue for females. c) Sex differences in FR calculated in ROIs where the interaction term is significant are reported. Asterisks indicate significant differences according to the paired signed rank test.*

4. Discussion

This study focuses on WM microstructural evolution in healthy aging as measured through both conventional and advanced DTI measures. Importantly, we found that females show, on average, a 14-year delay (relative to males) in the beginning of the FR-related changes in WM integrity, and that this result can be evidenced by using advanced diffusion imaging only (as compared to canonical DTI). All in all, FR show previously undisclosed sex and regionally-specific patterns of WM changes, consistent with converging observations from in multiple non-MRI domains and compatible with evolutionary theories (Chen and Maklakov, 2014).

Some previous studies have looked into the benefits of advanced multi-shell diffusion for characterizing brain microstructure in normal aging. Almost all of them used NODDI (Zhang et al., 2012), a multi-compartment model similar to CHARMED but based on lower diffusion weighting or b-value. While all studies show a similar effect of age on microstructural parameters (Billiet et al., 2015; Nazeri et al., 2015; Benitez et al. 2018; Fan et al., 2019), reported sex by age interactions are either not significant or inconsistent (Cox et al., 2015; Slater et al., 2019). Our work differs from published work in several aspects, notably: 1) we used a high b-value approach (CHARMED) to increase sensitivity to the restricted signal; 2) thanks to the large cohort and wide age range, we focus our analysis specifically on the age at which age-related changes begins; and 3) we tested the hypothesis that the interaction between sex and age plays a role in determining onset age.

4.1. Sex differences in the onset age of WM degeneration

While sex differences in WM have been reported using DTI (Kanaan et al. 2012) and are confirmed also by our study, interactions between sex and age reported to date are either no significant (Sullivan and Pfefferbaum, 2006) or small/inconsistent (Cox et al., 2015). Our study shows a significant difference of around 14-years in onset age estimated through FR between males and females. Previous DTI studies had found no sex-related

differences (Sullivan and Pfefferbaum, 2006), while multi-shell studies found small and inconsistent results (Cox et al., 2015). The strong sex differences that FR revealed may reflect known differences in the myelin trajectories between males and females. For example, it has been suggested that the promyelinating effects of female hormones may protect from age-related vulnerabilities in the myelination process (Bartzokis, 2004). Interestingly, transcriptomic data support this hypothesis: aging-related changes in gene expression are regionally and sexually dimorphic. In other words, females show age-related change in gene expression much later than males (between 80 and 90 years in females, between 60 and 70 years in males), especially in genes that regulate energy production and protein synthesis (Berchtold et al., 2008). A recent PET study looking at HDAC expression, an epigenetic enzyme family with critical importance to neural processes which plays a key role in myelination, has found significant gender differences (Gilbert et al., 2019).

Hence, we speculate that the striking differences in FR measures that we found between males and females in relation to aging reflect intrinsic and substantial sex-dependent variability in myelin protein synthesis and production during normal aging. Still, additional studies in post-mortem brains are needed to confirm this working hypothesis and to explore the intimate molecular, cellular, and physical bases that sustain the MRI signal contrast underlying the FR index.

4.2. Onset age across microstructural indices

Our combined skeleton and ROI-based statistical approach supports a quadratic relationship between age and the microstructural parameters in a number of WM areas. Specifically, the relationships between FA/FR and age follow an inverted U-shaped curve, showing an initial increase, possibly associated with evolving maturation, and a subsequent decrease, commonly associated with WM decline (Davis et al., 2009;

Kochunov et al. 2011; Lebel et al., 2012). As expected, diffusivity indices show an opposite trend. These changes parallel some known biological transformations underpinning WM evolution in lifespan (Kochunov et al. 2011); for example, it has been shown that WM myelination follows an approximately quadratic evolution, reaching its maximum around mid-life, and successively declining (Bartzokis et al., 2010). Additional age-related biological phenomena like neuronal cell death and low-grade chronic inflammation may help explaining the decline in diffusion MRI indices, including both canonical (FA, MD) and more advanced ones (FR). However, the precise relationship between neuroinflammation phenomena and diffusion MRI-based models remains to be determined.

Our study highlights that the WM decline estimated through FR begins much earlier (on average 2-5 years earlier, independent of sex) than the analogue decline estimated by FA and MD parameters. This difference is possibly due to the increased specificity to axonal integrity (which includes both myelination and axonal density) of the FR index compared to other DTI parameters (De Santis et al., 2019). Other studies have shown that multi-shell DTI is sensitive to progressive axonal loss both in lesions and normal appearing WM in early multiple sclerosis (De Santis et al., 2019; Toschi et al., 2019), the most common demyelinating disorder in the human brain (Love et al., 2005). Interestingly, we note that FR was particularly sensitive to age-related changes in the white-matter microstructural integrity in the PFC, especially the genu of the corpus callosum. The PFC and underlying WM tracts have been shown to undergo specific age- and gender-related modifications that are related to distinct cognitive and behavioral traits that characterize adolescence or normal and pathological ageing, often with marked sex differences (e.g., impulsivity, aggression behavioral disinhibition, etc.) (Weinstein and Dannon, 2015). In line with other studies (Billiet et al., 2015; Cox et al., 2016), only few

quadratic associations with age are found for FA, especially in the corpus callosum and in posterior regions. This might indicate a slower change over time, which needs to be better characterized collecting data with a wider range of age. All in all, the CHARMED axonal signal estimate FR can be positioned as a possible sensitive index for assessing changes in WM integrity, and holds promise as a novel biomarker in healthy and pathological aging.

4.3. Spatial gradients of WM degeneration

We also found a significant A-P gradient of WM degeneration in all indices (FA, MD and FR) which is in agreement with previous studies using canonical DTI indices (Bartzokis et al., 2012, Davis et al., 2009, Lebel et al., 2012, Salat et al., 2005). Together, these data are in keeping with and the 'retrogenesis' hypothesis (Bartzokis et al., 2012, Inano et al., 2011, Kumar et al., 2013, Lebel et al., 2012, Madden et al., 2004, Pfefferbaum et al., 2000, Salat et al., 2005) which posits that the WM fibers that myelinated latest during development (e.g., genu of corpus callosum) have thinner myelin sheaths relative to the WM tracts that myelinate earlier in development (e.g., splenium of corpus callosum). The same theory also sustains that this differential pattern of myelination results in a selective pattern of age-related vulnerability of the WM fibers, with the most anterior ones showing increased vulnerability compared with the most posterior ones.

In addition, in the present study, we also found a significant gradient in WM decline along the S-I direction for FR and MD; this novel finding is compatible with qualitative DTI findings in a cross-sectional cohort by Sullivan et al. (2010), who observed a trend in DTI indices measured in the superior versus inferior fiber tracts, as well as with the results of a longitudinal study of annual changes in DTI indices (Sexton et al.; 2014).

4.4. Strengths and limitations

Given the pivotal role of WM in healthy cognitive processing and in disease, characterizing its trajectories in normal aging is a fundamental preliminary step to better understand the pathological consequences of neurodegenerative disorders affecting WM. Our study highlights the utility of advanced diffusion MRI to characterize the WM microstructural integrity as well as its potential higher sensitivity to age- and sex-related effects relative to canonical DTI measures such as FA and MD. We believe that such novel diffusion techniques can become a promising early biomarker of WM integrity.

We also identified some limitations of our study. While the CHARMED model can provide enhanced sensitivity relatively to traditional DTI measures, the specific biological substrates that contribute to FR remain to be validated in biological and animal models and/or in ex-vivo investigations. Still, according to how the model is designed (Assaf et al., 2005), there are reasons to believe that the most likely substrate determining FR dynamics is represented by axonal integrity, in terms of both myelin content and inner axonal constituents. While other similar multi-compartment models are available (Fieremans et al, 2011; Zhang et al, 2012; Raffelt et al., 2017), we used CHARMED as our main hypothesis, informed by previous work (De Santis et al., 2017, De Santis et al., 2019, Toschi et al. 2019), was that FR is a better signature of axonal integrity compared to measures related to the hindered water population like those derived from DTI, and that its contribution is enhanced at higher b-values. While our results confirm the importance of acquiring high b-value datasets, future work is needed to decide which multi-compartment model is the most useful for such kind of data.

It should be noted that the cross-sectional nature of this study and the relatively small sample size (which is, however, fairly large compared to the majority of monocentric imaging studies) limits the generalizability of our findings, possibly due to between-subject variance and cohort effects, which should be verified in longitudinal

datasets and in larger populations. Furthermore, our DTI results might be not directly comparable to those reported in other studies due to different b-value ranges. It is also important to mention that additional factors other than sex could potentially influence the measured sex differences in WM integrity, as e.g. the cardiovascular health status; further studies are needed to characterize the interaction of such factors and / or comorbidities with brain aging trajectories. Finally, the quadratic models employed here are parsimonious mathematical approximations that capture age-related trends in microstructural parameters. The use of more versatile statistical models able (for example) to accommodate for different shapes and hence more degrees of freedom, might possibly lead to quantitatively different estimates of age of onset. However, the use of such models would most likely be more useful in significantly larger samples than the one employed here. Nevertheless, it is important to note that the onset age estimated here and in other studies should be only interpreted as a general indicator of a robust statistical effect rather than as the exact age at which the 'true' biological events take place (Murphy et al. 1996, Gur and Gur 2002, Goyal et al. 2019).

5 Conclusions

To summarize, FR (which is a sensitive proxy index for the combined effect of axonal and myelin integrity), has higher sensitivity than canonical DTI measures in detecting the age at which the WM microstructural components begin to change. This effect was particularly prominent in females, where the age-related WM decline was found to begin approximately 14 years later in comparison to males. Future studies are needed to replicate such findings in a longitudinal cohort of healthy aging individuals. Additionally, studies in clinical populations will allow to test the hypothesis that FR measures are able to robustly identify early changes in WM characteristic of neurodegenerative disorders.

References

Assaf Y, Basser PJ. Composite hindered and restricted model of diffusion (CHARMED) MR imaging of the human brain. Neuroimage 2005;27:48–58.

Barazany D, Basser PJ, Assaf Y. In vivo measurement of axon diameter distribution in the corpus callosum of rat brain. Brain 2009;132, 1210–1220.

Bartzokis G. Quadratic trajectories of brain myelin content: Unifying construct for neuropsychiatric disorders. Neurobiology of Aging 2004;25:49-62.

Bartzokis G, Lu PH, Tingus K, Mendez MF, Richard A, Peters DG, Oluwadara B, Barrall KA, Finn JP, Villablanca P, Thompson PM, Mintz J. Lifespan trajectory of myelin integrity and maximum motor speed. Neurobiology of Aging 2010;31:1554-1562.

Basser PJ, Mattiello J, LeBihan D. Estimation of the effective self-diffusion tensor from the NMR spin echo. J Magn Reson B 1994;103:247–254.

Benitez A, Jensen JH, Falangola MF, Nieterte PJ, Helpern JA. Modeling white matter tract integrity in aging with diffusional kurtosis imaging. Neurobiol Aging 2018;70:265–275.

Berchtold NC, Cribbs DH, Coleman PD, Rogers J, Head E, Kim R, Beach T, Miller C, Troncoso J, Trojanowski JQ, Zielke HR, Cotman CW. Gene expression changes in the course of normal brain aging are sexually dimorphic. Proc Natl Acad Sci USA 2008;105:15605–15610.

Billiet T, Vandenbulcke M, Mädler B, Peeters R, Dhollander T, Zhang H, Deprez S, Van den Bergh BR, Sunaert S, Emsell L. Age-related microstructural differences quantified using myelin water imaging and advanced diffusion MRI. Neurobiology of Aging 2015;36:2107-2121.

Chang LC, Jones DK, Pierpaoli C. RESTORE: robust estimation of tensors by outlier rejection. Magn Reson Med 2005;53:1088-95.

Chen HY, Maklakov AA. Condition dependence of male mortality drives the evolution of sex differences in longevity. Curr Biol. 2014;24:2423-7.

Coutu JP, Chen JJ, H. Rosas D, Salata DH. Non-Gaussian water diffusion in aging white matter. Neurobiol Aging 2014;35:1412–1421.

Cox SR, Ritchie SJ, Tucker-Drob EM, Liewald DC, Hagenaars SP, Davies G, Wardlaw JM, Gale CR, Bastin ME, Deary IJ. Ageing and brain white matter structure in 3,513 UK Biobank participants. Nature Comm. 2015;7:13629

Davis SW, Dennis NA, Buchler NG, White LE, Madden DJ, Cabeza R. Assessing the effects of age on long white matter tracts using diffusion tensor tractography. Neuroimage 2009;46:530–541.

de Groot M, Cremers LG, Ikram MA, Hofman A, Krestin GP, van der Lugt A, Niessen WJ, Vernooij MW. White Matter Degeneration with Aging: Longitudinal Diffusion MR Imaging Analysis. Radiology 2016;279:532-41.

De Santis S, Assaf Y, Jones DK.. Using the biophysical CHARMED model to elucidate the underpinnings of contrast in diffusional kurtosis analysis of diffusion-weighted MRI. Magn Reson Mater Phy 2012;25:267–276.

De Santis S, Granberg T, Ouellette R, Treaba CA, Herranz E, Fan Q, Mainero C, Toschi N. Early axonal damage in normal appearing white matter in Multiple Sclerosis: novel insights from multi-shell diffusion MRI. Neuroimage:Clinical 2019;22:101699.

Fan Q, Tian Q, Ohringer NA, Nummenmaa A, Witzel T, Tobyne SM, Klawiter EC, Mekkaoui C, Rosen BR, Wald LL, Salat DH, Huang SY. Age-related alterations in axonal microstructure in the corpus callosum measured by high-gradient diffusion MRI. Neuroimage 2019;191:325-336.

Fieremans E, Jensen JH, Helpern JA. White matter characterization with diffusional kurtosis imaging. Neuroimage. 2011 Sep 1;58(1):177-88.

Filley CM, Fields RD. White matter and cognition: making the connection. J Neurophysiol 2016;116:2093-2104.

Franceschi C, Capri M, Monti D, Giunta S, Olivieri F, Sevini F, Panourgia MP, Invidia L, Celani L, Scurti M, Cevenini E, Castellani GC, Salvioli S. Inflammaging and anti-inflammaging: a systemic perspective on aging and longevity emerged from studies in humans. Mech Ageing Dev 2007;128:92-105.

Gilbert TM, Zürcher NR, Catanese MC, Tseng CJ, Di Biase MA, Lyall AE, Hightower BG, Parmar AJ, Bhanot A, Wu CJ, Hibert ML, Kim M, Mahmood U, Stufflebeam SM, Schroeder FA, Wang C, Roffman JL, Holt DJ, Greve DN, Pasternak O, Kubicki M, Wey H-Y, Hooker JM. Neuroepigenetic signatures of age and sex in the living human brain. Nature Communications 2019;10: 2945

Goyal MS, Blazey TM, Su Y, Couture LE, Durbin TJ, Bateman RJ, Benzinger TLS, Morris JC, Raichle ME, Vlassenko AG. Persistent metabolic youth in the aging female brain. Proc Natl Acad Sci USA 2019;116:3251-3255.

Goveas J, O'Dwyer L, Mascalchi M, Cosottini M, Diciotti S, De Santis S, Passamonti L, Tessa C, Toschi N, Giannelli M. Diffusion-MRI in neurodegenerative disorders. Magn Reson Imaging. 2015;33:853-76.

Gur RE, Gur RC. Sex differences in aging: cognition, emotions, and neuroimaging studies. Dialogues Clin Neurosci 2002;4:197–210.

Kanaan RA, Allin M, Picchioni M, Barker GJ, Daly, Shergill SE, Woolley J, McGuire PK. Sex Differences in White Matter Microstructure. PLoS One 2012;7:e38272.

Kemper, T. L. (1994). Neuroanatomical and neuropathological changes during aging and dementia. In M. L. Albert & J. E. Knoefel (Eds.), Clinical neurology of aging (pp. 3-67). New York, NY, US: Oxford University Press.

Klein A, Andersson J, Ardekani BA, Ashburner J, Avants B, Chiang MC, Christensen GE, Collins DL, Gee J, Hellier P, Song JH, Jenkinson M, Lepage C, Rueckert D, Thompson P, Vercauteren T, Woods RP, Mann JJ, Parsey RV. Evaluation of 14 nonlinear deformation algorithms applied to human brain MRI registration. Neuroimage 2009;46:786-802.

Kochunov P, Glahn DC, Lancaster J, Thompson PM, Kochunov V, Rogers B, Fox P, Blangero J, Williamson DE. Fractional anisotropy of cerebral white matter and thickness of cortical gray matter across the lifespan. Neuroimage 2011;58:41-49.

Kuo LW, Chen JH, Wedeen VJ, Tseng WY. Optimization of diffusion spectrum imaging and q-ball imaging on clinical MRI system. Neuroimage 2008;41:7-18.

Lebel C, Gee M, Camicioli R, Wieler M, Martin W, Beaulieu C. Diffusion tensor imaging of white matter tract evolution over the lifespan. Neuroimage 2012;60:340-52.

Leemans A, Jeurissen B, Sijbers J, Jones DK. ExploreDTI: a graphical toolbox for processing, analyzing, and visualizing diffusion MR data, 2009 In 17th annual meeting of International Society for Magnetic Resonance in Medicine Berkeley, CA, USA.

Lotze M, Domin M, Gerlach FH, Gaser C, Lueders E, Schmidt CO, Neumann N. Novel findings from 2,838 Adult Brains on Sex Differences in Gray Matter Brain Volume. Scientific Reports 2019; 9:1671

Love S. Demyelinating diseases. J Clin Pathol 2006;59:1151–1159.

Mattson MP, Magnus T. Aging and Neuronal Vulnerability. Nat Rev Neurosci 2006;7:278–294.

Miller DJ, Duka T, Stimpson CD, Schapiro SJ, Baze WB, McArthur MJ, Fobbs AJ, Sousa AM, Šestan N, Wildman DE, Lipovich L, Kuzawa CW, Hof PR, Sherwood CC. Prolonged myelination in human neocortical evolution. Proc Natl Acad Sci USA 2012;109: 16480–16485.

Mori S, Oishi K, Jiang H, Jiang L, Li X, Akhter K, Hua K, Faria AV, Mahmood A, Woods R, Toga AW, Pike GB, Neto PR, Evans, A, Zhang J, Huang H, Miller MI, van Zijl P, Mazziotta J. Stereotaxic white matter atlas based on diffusion tensor imaging in an icbm template. Neuroimage 2008;40:570–582.

Murphy DG, DeCarli C, McIntosh AR, Daly E, Mentis MJ, Pietrini P, Szczepanik J, Schapiro MB, Grady CL, Horwitz B, Rapoport SI. Sex differences in human brain morphometry and metabolism: an in vivo quantitative magnetic resonance imaging and positron emission tomography study on the effect of aging. Arch Gen Psychiatry 1996;53:585-94.

Nazeri A, Chakravarty M, Rotenberg DJ, Rajji TK, Rathi Y, Michailovich OV, Voineskos AN. Functional Consequences of Neurite Orientation Dispersion and Density in Humans across the Adult Lifespan. J Neurosci. 2015 Jan 28; 35(4): 1753–1762.

Raffelt DA, Tournier JD, Smith RE, Vaughan DN, Jackson G, Ridgway GR, Connelly A. Investigating white matter fibre density and morphology using fixel-based analysis. Neuroimage. 2017 Jan 1;144(Pt A):58-73.

Peters R. Ageing and the brain. Postgrad Med J. 2006;82:84–88.

Ritchie SJ, Cox SR, Shen X, Lombardo MV, Reus LM, Alloza C, Harris MA, Alderson HL, Hunter S, Neilson E, Liewald DCM, Auyeung B, Whalley HC, Lawrie SM, Gale CR, Bastin ME, McIntosh AM, Deary IJ. Sex Differences in the Adult Human Brain: Evidence from 5216 UK Biobank Participants. Cereb Cortex 2018;28(8):2959-2975.

Salat DH, Buckner RL, Snyder AZ, Greve DN, Desikan RS, Busa E, Morris JC, Dale AM, Fischl B. Thinning of the cerebral cortex in aging. Cereb Cortex 2004;14:721-30.

Sexton CE, Walhovd KB, Storsve AB, Tamnes C, Westlye LT, Joansen-Berg H, Fjell AM. Accelerated changes in white matter microstructure during aging: a longitudinal diffusion tensor imaging study. J Neurosci 2014;34:15425-36.

Slater DA, Melie-Garcia L, Preisig M, Kherif F, Lutti A, Draganski B. Evolution of white matter tract microstructure across the life span. Hum Brain Mapp. 2019 May;40(7):2252-2268.

Smith SM, Jenkinson M, Johansen-Berg H, Rueckert D, Nichols TE, Mackay CE, Watkins KE, Ciccarelli O, Cader MZ, Matthews PM, Behrens TE. Tract-based spatial statistics: Voxelwise analysis of multi-subject diffusion data. NeuroImage 2006;31:1487-1505.

Sullivan EV, Pfefferbaum A. Diffusion tensor imaging and aging. Neuroscience and Biobehavioral Reviews 2006;30:749-761.

Sullivan EV, Rohlfing T, Pfefferbaum A. Longitudinal study of callosal microstructure in the normal adult aging brain using quantitative DTI fiber tracking. Dev Neuropsychol 2010a;35:233-56.

Sullivan EV, Rohlfing T, Pfefferbaum A. Quantitative fiber tracking of lateral and interhemispheric white matter systems in normal aging: relations to timed performance. Neurobiol Aging 2010b;3:464-81.

Szafer A, Zhong JH, Gore JC. Theoretical model for water diffusion in tissues. Magn Reson Med 1995;33:697-712.

Tavor I, Hofstetter S, Assaf Y. Micro-structural assessment of short term plasticity dynamics. Neuroimage. 2013;81:1-7.

van Gelderen P, DesPres D, van Zijl PC, Moonen CT. Evaluation of restricted diffusion in cylinders. Phosphocreatine in rabbit leg muscle. J Magn Reson B. 1994 Mar;103(3):255-60.

Weinstein A, Dannon P. Is Impulsivity a Male Trait Rather than Female Trait? Exploring the Sex Difference in Impulsivity. Curr Behav Neurosci Rep 2015;2: 9-14.

Xie S, Zhang Z, Chang F, Wang Y, Zhang Z, Zhou Z, Guo H. Subcortical White Matter Changes with Normal Aging Detected by Multi-Shot High Resolution Diffusion Tensor Imaging. PLoS One 2016;11:e0157533.

Yang S, Li C, Zhang W, Wang W, Tang Y. Sex differences in the white matter and myelinated nerve fibers of Long-Evans rats. Brain Res 2008;1216:16-23.

Yeh FC, Tseng WY. NTU-90: a high angular resolution brain atlas constructed by q-space diffeomorphic reconstruction. Neuroimage 2011;58:91-99.

Zhang H, Schneider T, Wheeler-Kingshott CA, Alexander DC. NODDI: practical in vivo neurite orientation dispersion and density imaging of the human brain. Neuroimage, 2012;61:1000-1016.

NEW:

Yakovlev PL, Lecours AR. The myelogenetic cycles of regional maturation of the brain. In: Resional development of the brain in early life (Minkowski A, eds), 1967, pp 3-70. Oxford: Blackwell.

Beaulieu, C., 2002. The basis of anisotropic water diffusion in the nervous system—a technical review. NMR Biomed. 2002;15:435-455.

De Santis S, Drakesmith M, Bells S, Assaf Y, Jones DK. Why diffusion tensor MRI does well only some of the time: variance and covariance of white matter tissue microstructure attributes in the living human brain. Neuroimage 2014;89:35-44.

De Santis S, Granberg T, Ouellette R, Treaba CA, Qiuyun Fan, Herranz E, Mainero C, Toschi N. Early axonal damage in normal appearing white matter in multiple sclerosis: Novel insights from multi-shell diffusion MRI. Conf Proc IEEE Eng Med Biol Soc. 2017:3024-3027.

Toschi N, De Santis S, Granberg T, Ouellette R, Treaba CA, Herranz E, Mainero C. Evidence for Progressive Microstructural Damage in Early Multiple Sclerosis by Multi-Shell Diffusion Magnetic Resonance Imaging. Neuroscience 2019;403:27-34.

Inano S, Takao H, Hayashi N, Abe O, Ohtomo K. Effects of age and gender on white matter integrity. AJNR Am J Neuroradiol 2011;32(11):2103-9.

Kumar R, Chavez AS, Macey PM, Woo MA, Harper RM. Brain axial and radial diffusivity changes with age and gender in healthy adults. Brain Res. 2013;1512:22-36.

Madden DJ, Whiting WL, Huettel SA, White LE, MacFall JR, Provenzale JM. Diffusion tensor imaging of adult age differences in cerebral white matter: relation to response time. Neuroimage 2004;21:1174–1181

Pfefferbaum A, Sullivan EV, Hedehus M, Lim KO, Adalsteinsson E, Moseley M. Age-related decline in brain white matter anisotropy measured with spatially corrected echo-planar diffusion tensor imaging. Magn Reson Med. 2000;44:259-68.